Research Article

Chemical Review and Letters
journal homepage: www.chemrevlett.com
ISSN (online): 2645-4947 (print) 2676-7279

Terephthalate-based metal-organic frameworks as corrosion inhibitors for AM60B magnesium alloy in ethylene glycol solution

Soheila Mohamadian-Kalhor[a], Ladan Edjlali[a], Hadi Basharnavaz[b], and Moosa Es'haghi*[, a]

[a]*Department of Chemistry, Tabriz Branch, Islamic Azad University, Tabriz, Iran*
[b]*Department of Chemistry, Faculty of Science, University of Mohaghegh Ardabili, P.O. Box 179, Ardabil, Iran*

ARTICLE INFO

Article history:
Received 26 May 2021
Received in revised form 14 July 2021
Accepted 15 July 2021
Available online 20 July 2021

Keywords:
Metal-organic frameworks; Terephthalate; Corrosion; Electrochemical impedance spectroscopy; Magnesium alloy; Ethylene glycol.

ABSTRACT

A series of metal-organic frameworks (MOFs), including aluminum terephthalate (AlTp), bismuth terephthalate (BiTp), and chromium terephthalate (CrTp), was synthesized for use as inhibitors to protect AM60B magnesium alloy from corrosion in 30% ethylene glycol solution containing 0.5 M NaCl. The prepared MOFs were characterized using the X-ray diffraction (XRD) spectrum, Brunauer, Emmett, and Teller (BET), and scanning electron microscope (SEM) images. Electrochemical impedance spectroscopy (EIS) and potentiodynamic polarization were applied to evaluate the inhibition performance of the MOFs in a concentration range of 50-400 ppm. Inhibition efficiencies of 84.17%, 86.52%, and 89.64% were obtained for BiTp, AlTp, and CrTp at an optimum concentration of 200, 400, and 400 ppm, respectively, indicating high potentials of the proposed inhibitors. Gibbs free energy of adsorption obtained for BiTp, AlTp, and CrTp were as -30.016, -26.725, and -25.792 kJ mol-1, respectively. These results revealed that the inhibitors were adsorbed on the metal surface through both physisorption and chemisorption processes.

1. Introduction

Magnesium alloys have some features, such as light density, good mechanical properties, and high strength-to-weight ratio that make them promising alternatives to aluminum and steel alloys for automotive, aerospace, and electronic applications. In automotive industries, a magnesium engine block has been targeted that can significantly reduce the weight and fuel consumption of an automobile. In the cooling system of such an engine block, corrosion is always a significant problem. It was demonstrated that many existing commercial coolants exhibit no adequate corrosion inhibition to magnesium alloys [1,2]. To solve this problem, inhibitors are usually included in most brands of commercial coolants, where the main components of a conventional coolant are 30 vol% ethylene glycol + 70 vol% H2O, and the added inhibitors include phosphate, molybdate, nitrate, borate, nitrite, silicate, and benzoate [3]. It should be noted that although the application of corrosion inhibitors is the simplest way to protect metals in an aqueous environment, their usage for the protection of magnesium alloys maybe not a proper method because of the tendency of Mg to localized corrosion [4]. The protection of AZ91 Mg alloy by organic-inorganic hybrid coatings has recently been reported as an effective procedure [5–11]. However, in the case of cooling systems of vehicles, the addition of corrosion inhibitors is strongly recommended [12–14]. It was reported that the Mg alloys corrosion rate in aqueous ethylene glycol solutions is dependent on the concentration of the solution [3]. A diluted solution is more corrosive than a concentrated one. Additionally, an ethylene glycol solution contaminated by individual contaminants such as NaCl was found to be strongly corrosive to Mg alloys. A literature survey shows that the number of studies performed on the corrosion resistance of Mg alloys in ethylene glycol solutions is so limited [3,4,12,13]. On this basis, in the present work, we introduce a series of metal-organic frameworks (MOFs) to inhibit the AM60B magnesium alloy in ethylene glycol solution containing 0.5 M NaCl. MOFs are a promising class of components

* Corresponding author.; e-mail: eshaghi.m@iaut.ac.ir

that have attracted much attention for their potential applications. Their structure is characterized by metal clusters and organic linkers. Having polar groups and large surface areas could make these materials proper candidates for corrosion inhibition. As far as our knowledge is concerned, there is no report published on the use of MOFs as corrosion inhibitors in the coolant. Thus, results obtained here could hopefully help draw an overall inference about the performance of MFOs in ethylene glycol solution for the active protection of magnesium.

2. Results and Discussion

2.1. Characterization of MOFs

XRD patterns of the BiTp, AlTp, and CrTp are shown in Fig.1. This figure demonstrated the crystalline structures of the prepared MOFs. Some main diffraction peaks of the AlTp appeared at 2θ= 9.48°, 12.55°, 17.92°, 23.32°, 25.12°, and 27.28° [15]. BiTp exhibited its main diffraction peaks at 2θ = 5.48°, 7.27°, 18.81°, 26.98°, 32.31°, and 46.21°, which were consistent with data reported in the literature [16]. In the case of CrTp, characteristic peaks appeared at 2θ = 8.69°, 9.31°, 16.77°, and 19.15°, which were in agreement with data reported previously [17,18].

SEM images of the synthesized MOFs are shown in Fig. 2. It is observed that they are entirely different in shape. Accordingly, the AlTp species appear as layered cubes with small pores. The thickness of such layers in some areas is 20-60 nm. Sharp edges and directional fractures indicate the high crystallinity of the AlTp. The CrTp particles show an octagonal morphology with sharp edges and fine porosity. The length of the base on each side is found to be 300-500 nm. The BiTp is seen as filamentous particles with a size distribution of 40-90 nm and fine porosity.

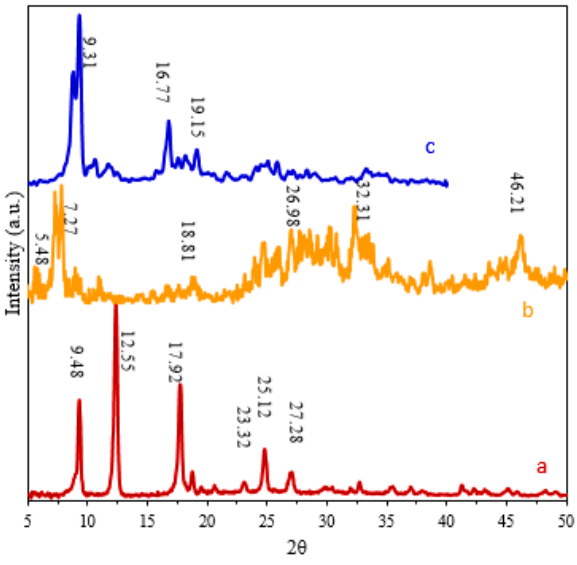

Fig.1. XRD patterns of AlTp (a), BiTp (b), and CrTp (c).

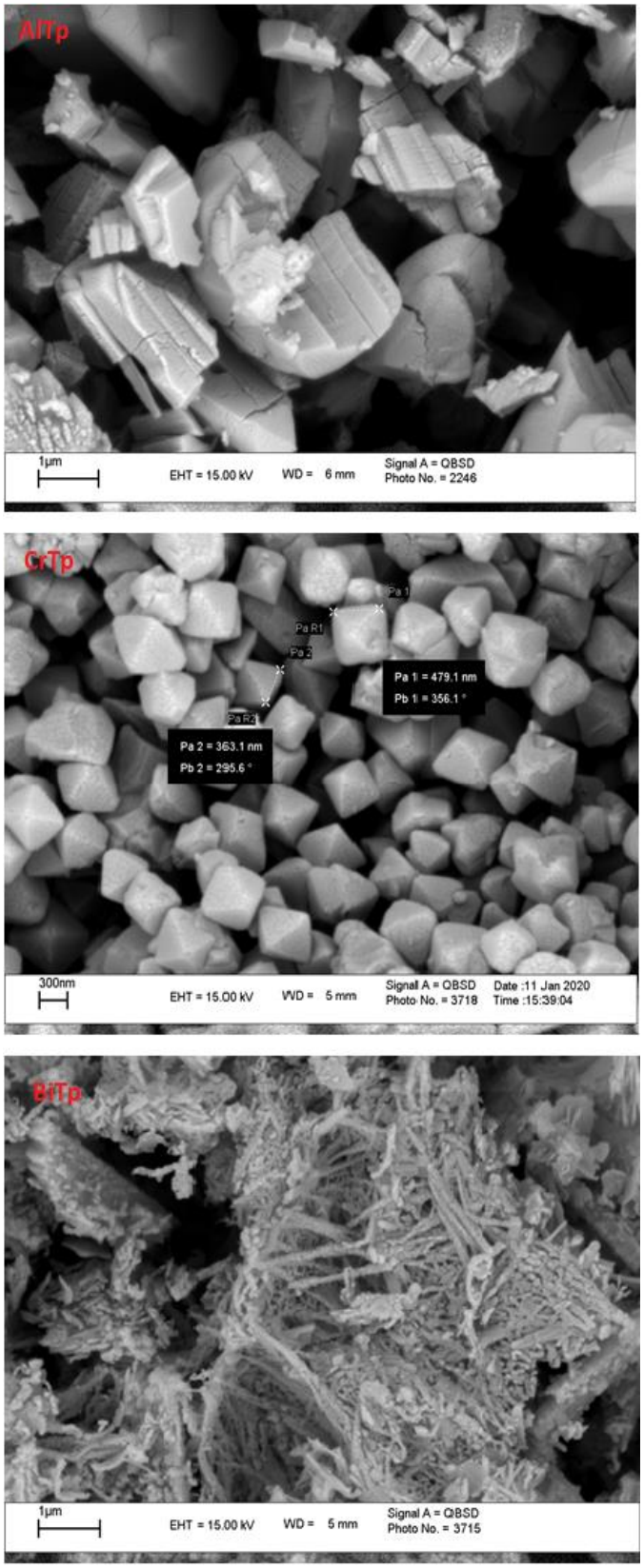

Fig. 2. SEM images of the synthesized MOFs

2.2. Potentiodynamic polarization

Potentiodynamic polarization measurements were carried out for the AM60B alloy in an aqueous ethylene glycol solution. The corresponding plots in the absence and

presence of various contents of inhibitors are depicted in Fig. 3.

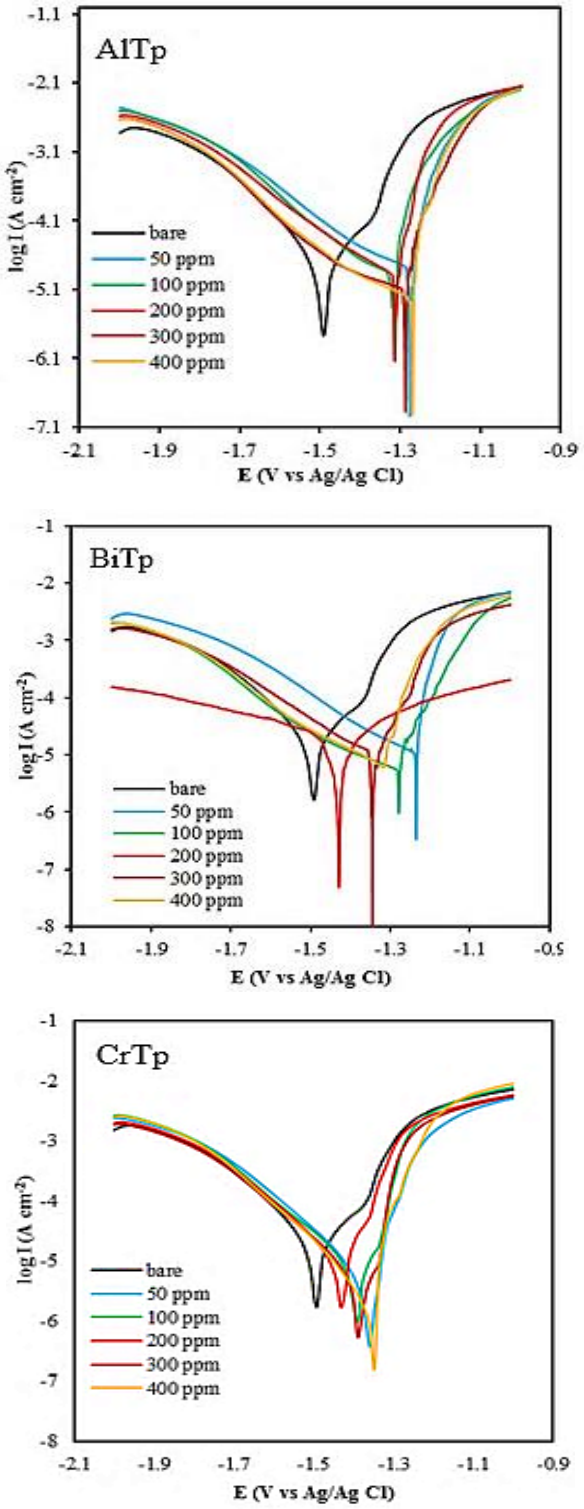

Fig. 3. Potentiodynamic polarization plots of the AM60B alloy in 30% ethylene glycol solution in the presence of MOFs

Corrosion potential (Ecorr) and corrosion current density (Icorr) were determined from polarization curves by Tafel extrapolation. Data obtained are given in Table 1. It is well known that I_{corr} is a kinetic parameter indicating corrosion rate. Table 1 revealed that I_{corr} in blank solution was much higher than those in solutions containing MOF. For instance, I_{corr} value decreased from 17.11 µA cm^2 in the blank solution to 1.99 µA cm^2 in the presence of 400 ppm CrTp.

Table 1. Polarization parameters

Inhibitor	Con. (ppm)	E (V)	I (µA cm^{-2})	IE %
Bare	-	-1.39	5.96	-
AlTp	50	-1.28	8.33	51.32
	100	-1.31	7.72	54.88
	200	-1.31	7.33	57.16
	300	-1.29	5.75	66.39
	400	-1.28	3.17	81.47
BiTp	50	-1.23	7.54	55.93
	100	-1.28	4.53	73.52
	200	-1.43	3.37	80.30
	300	-1.34	4.07	76.21
	400	-1.32	5.97	65.11
CrTp	50	-1.35	5.86	65.75
	100	-1.40	5.11	70.13
	200	-1.43	4.24	75.22
	300	-1.36	3.89	77.26
	400	-1.35	1.99	88.37

Such a result indicated that the proposed MOFs were effective to reduce the corrosion of magnesium. Corrosion mitigation was due to the adsorption of inhibitor molecules on the AM60B surface. This type of adsorption was mainly due to the presence of the O=C–O- group in the terephthalate structure, providing an active site to attach to the metal surface. A charge transfer between the adsorbed molecule and the surface plays a critical role in the corrosion inhibition process. Such a charge transfer could happen between the empty 2π* state of the carboxyl group in terephthalate and the Mg-2s states of the metal [6]. Table 1 showed that the I_{corr} values of the AM60B alloy increased with increasing the MOF concentration. This was an indication of increased adsorbed molecules on the metal surface at higher concentrations. Inhibition efficiencies (η) included in Table 1 are calculated by the following equation[19]:

$$\eta = \frac{I^0_{corr} - I_{corr}}{I^0_{corr}} \times 100 \qquad (1)$$

where I^0_{corr} and I_{corr} are corrosion current densities in blank and inhibited solutions, respectively. Maximum values were obtained as 80.30%, 81.5%, and 88.37% in the presence of BiTp, AlTp, and CrTp, respectively. The inspection of Table 1 indicated that E_{corr} had a value of -1.49 V in the blank solution, whereas it shifted to more positive values in the presence of MOFs. Such a replacement was a consequence of inhibitor adsorption on the Mg surface, leading to the formation of a barrier against corrosive agents. Furthermore, polarization curves showed that the addition of MOF affected anodic branches more than cathodic ones. This may indicate that the proposed inhibitors reduced corrosion mainly by decreasing the rate of metal dissolution reaction.

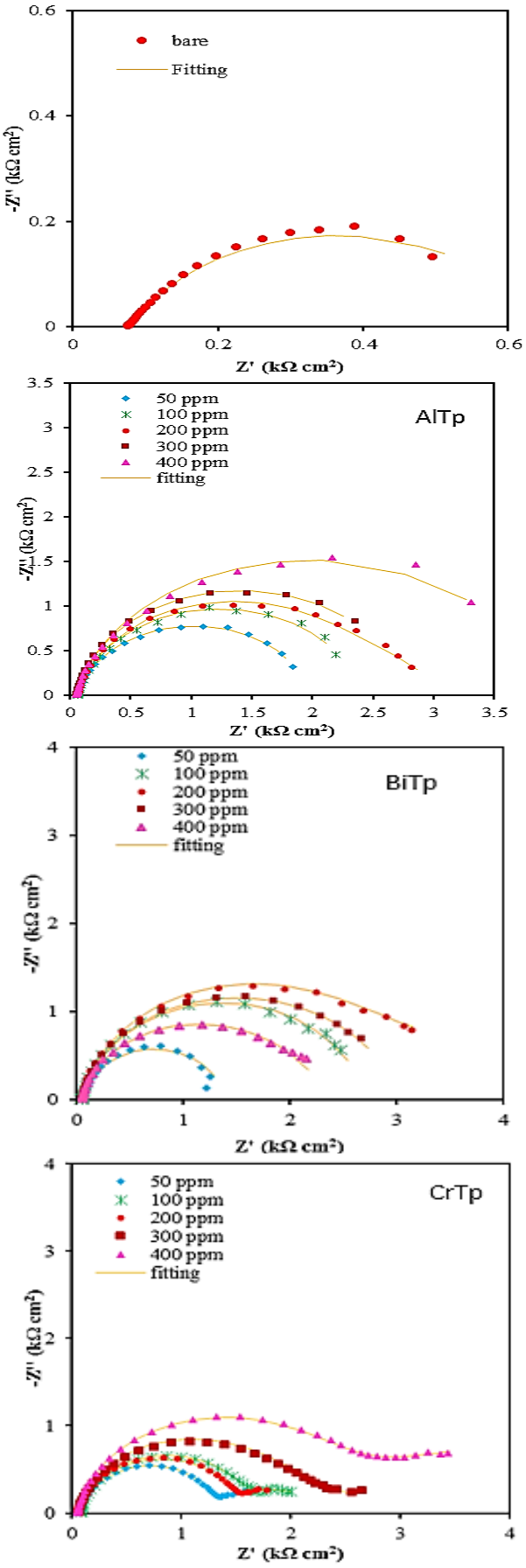

Fig. 4. Nyquist diagrams of the AM60B alloy in 30% ethylene glycol solution in the absence and presence of MOFs.

2.3. EIS results

Fig.4 depicts the EIS spectra of the AM60B alloy after 2 h immersion in the corrosive solution (30% ethylene glycol+ 70% water containing 0.5 M NaCl) containing inhibitors. Accordingly, Nyquist diagrams illustrate two characteristic loops, which are related to two specific time constants. The low-frequency time constant is attributed to the Faradic charge transfer process at the electrolyte/AM60B interface, and the high-frequency time constant could be assigned to capacitance and the resistance of the oxide film on the metal surface. An equivalent circuit shown in Fig.5 was applied to assess EIS data. In this circuit, CPE_f is the constant phase element and R_f is the resistance of the oxide layer. CPE_{dl} is the double-layer capacitance of the oxide layer/metal interface, and R_{ct} is charge transfer resistance. The CPE applied instead of a pure capacitor contains two specific parameters: Y (constant of the CPE) and n (exponent of the CPE with a value between 0 and 1)[20,21]. The CPE impedance and R_{total} (sum of the charge transfer resistance and oxide layer resistance) are calculated based on the following equations[22]:

$$Z_{CPE} = (j\omega C)^{-n} \quad (2)$$

$$R_{total} = R_f + R_{ct} \quad (3)$$

where Z, j, ω, C and n are the impedance, square root of −1, angular frequency, capacitance, and measure of the non-ideality of the capacitor.

Table 2 contains various parameters achieved from fitting EIS spectra by Zview2 software. Furthermore, R_{total} values were used to calculate inhibition efficiencies (IE%) using the following equation[23]:

$$IE\% = \frac{R_{total} - R^0_{total}}{R_{total}} \times 100 \quad (4)$$

where R_{total} and R^0_{total} are the sum of the charge transfer resistance and oxide layer resistance in inhibited and uninhibited solutions, respectively.

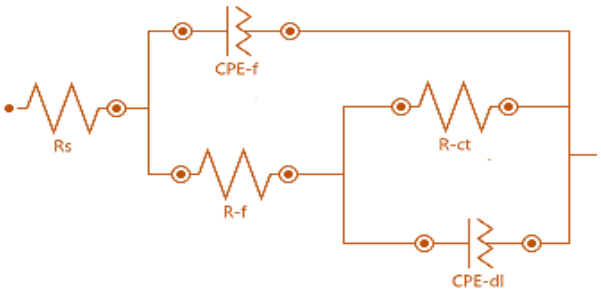

Fig. 5. Equivalent circuit used to fit experimental EIS data.

According to Eq. (4), inhibition efficiencies of the BiTp, AlTp, and CrTp were achieved as 84.17%, 86.52%, and 89.64% at an optimum concentration of 200, 400, and 400 ppm, respectively. Such high potentials of the proposed inhibitors could be explained by the presence of π-rich systems and lone pair electrons of O atoms, which strongly interact with the metal surface [24,25]. The active surface of each inhibitor that is available to interact with the metal surface can be considered as a parameter affecting inhibition performance (Table3). On this basis, it could be expected that inhibitors with higher active surface areas exhibit better inhibition efficiencies. BET data revealed that the active surfaces of the studied MOFs were in the order BiTp < AlTp < CrTp. Such a trend that was in agreement with IE% results indicated that the AlTp and CrTp particles with cubic and octagonal morphologies provided higher corrosion mitigation than the BiTp with a filamentous structure and an active surface area of just 11 m^2 g^{-1}.

Inhibitor adsorption on the metal surface and inhibitor-metal interactions can be studied by adsorption isotherms. For this purpose, EIS data were used to obtain surface coverage (θ=(IE%)/100) and, in turn, the adsorption mechanism of inhibitor on the AM60B alloy surface. To find a proper adsorption isotherm, Temkin, Freundlich, and Langmuir isotherms were tried to fit experimental data. Results showed that the Langmuir isotherm best described the adsorption process. This isotherm can be expressed by the following equation[26,27]:

$$\frac{C_{inh}}{\theta} = C_{inh} + \frac{1}{K_{ads}} \quad (5)$$

where C_{inh} is the inhibitor concentration, and K_{ads} is the equilibrium constant for the adsorption-desorption process. Fig.6 shows plots of C_{inh}/θ versus Cinh. The plot intercept can be used to determine K_{ads} values, which were attained as 0.1815, 0.0481, and 0.0330 L mg^{-1} for BiTp, AlTp, and CrTp, respectively. Gibbs free energy of inhibitor adsorption on the AM60B surface was calculated using the following equation[28]:

$$\Delta G_{ads} = -RT\ln(55.5K_{ads}) \quad (6)$$

where 55.5 is the molar concentration of water, which is replaced by 106 when inhibitor concentration is in ppm [29]. ΔG_{ads} values obtained for BiTp, AlTp, and CrTp were as -30.016, -26.725, and -25.792 kJ mol^{-1}, respectively. It is generally proposed that when ΔG_{ads} has a value up to -20 kJ mol^{-1} or lower, inhibitor molecules are adsorbed on the metal surface via electrostatic interactions, and it is considered as a physisorption process. On the other hand, ΔG_{ads} with a value of more than -40 kJ mol^{-1} shows that inhibitor molecules are adsorbed on the surface through charge sharing between the inhibitor and the metal, and adsorption is considered as a chemisorption process[30,31]. ΔG_{ads} values obtained for the inhibitors investigated were between the above two values, implying that the adsorption mechanism of inhibitors involved two types of interaction, chemisorption, and physisorption.

Table 2. EIS parameters obtained from fitting experimental data. The immersion time before all measurements was about 2 h

Inhibitors	Con. (ppm)	CPE_f		R_f (kΩ.cm^2)	CPE_{dl}		R_{ct} k(Ω.cm^2)	R_f+R_{ct} (kΩ.cm^2)	IE%	Fitting Error
		$Y_0\times10^{-6}$ ($\Omega^{-1}cm^{-2}S^n$)	n		$Y_0\times10^{-6}$ ($\Omega^{-1}cm^{-2}S^n$)	n				
Bare	-	255.13	0.72	0.012	417028	0.66	0.566	0.578	-	0.0001
AlTp	50	6.06	0.87	1.911	8.04	0.86	0.019	1.930	70.05	0.0003
	100	10.29	0.85	2.323	3.00	0.94	0.024	2.347	75.37	0.0005
	200	11.37	0.64	2.669	8.07	0.93	0.024	2.693	78.54	0.0002
	300	6.22	0.88	2.705	5.17	0.93	0.015	2.720	78.75	0.0006
	400	12.39	0.68	4.274	7.03	0.94	0.014	4.288	86.52	0.0007
BiTp	50	11.35	0.91	1.244	9.80	0.91	0.090	1.334	56.67	0.0003
	100	9.97	0.81	2.646	5.19	0.96	0.016	2.662	78.29	0.0009
	200	19.81	0.51	3.559	8.77	0.94	0.093	3.652	84.17	0.0000
	300	10.14	0.92	3.029	14.25	0.53	0.038	3.067	81.15	0.0001
	400	20.00	0.61	2.317	7.54	0.95	0.027	2.344	75.34	0.0011
CrTp	50	13.99	0.90	1.262	2528.20	0.80	0.695	1.957	70.46	0.0008
	100	14.61	0.89	1.571	1735.10	0.80	0.591	2.162	73.27	0.0005
	200	14.62	0.89	1.469	2469.10	0.76	0.779	2.248	74.29	0.0004
	300	13.07	0.89	1.868	663.91	0.54	0.868	2.736	78.87	0.0003
	400	12.78	0.89	2.445	765.33	0.52	3.133	5.578	89.64	0.0003

Table 3. Data obtained from BET analysis of the synthesized MOFs.

MOF	Active surface (m^2 g^{-1})	Pore size (nm)	Pore volume (cm^3 g^{-1})
AlTp	975.72	2.00	0.49
BiTp	11.04	4.82	0.013
CrTp	2731.00	2.12	1.45

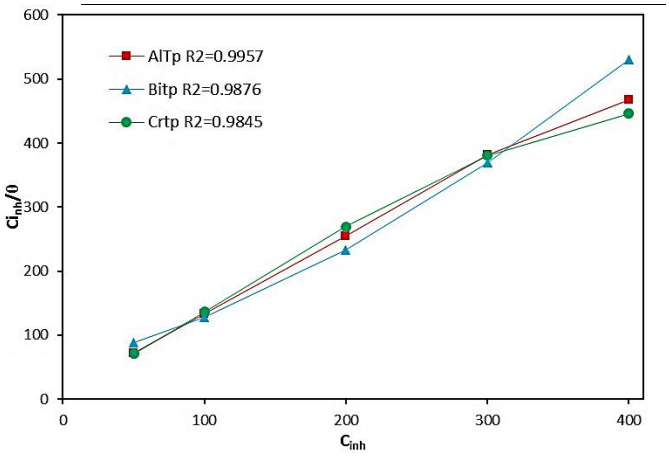

Fig. 6. Langmuir isotherm to describe the adsorption process of the synthesized MOFs on the metal surface.

3. Experimental

3.1. Materials and apparatus

All materials and solvents were purchased from Merck Co. and used without purification. The purity of the materials was terephthalic acid (98%), HNO_3 (65%), $Al(NO_3)_3.9H_2O$ (99%), $Cr(NO_3)_3.9H_2O$ (99%), $Bi(NO_3)_3.5H_2O$ (98%), and Ethylene glycol anhydrous (99.8%). XRD patterns were obtained using Philips (X-Pro) in a scan range of 2θ=5-70°. The morphology of synthesized MOFs was investigated by providing SEM images via LEO 1430VP. BET data were obtained using Belsorp II at 77 K.

3.2. Synthesis of MOFs

To synthesize aluminum terephthalate MOF under hydrothermal conditions, 45 mmol $Al(NO_3)_3.9H_2O$ and 22.5 mmol terephthalic acid were mixed in 65 ml deionized water with a magnetic stirrer for 10 min and transferred to a PTF Teflon reactor. The pH of the mixture was adjusted to 2–3 by adding concentrated HNO_3. The Teflon reactor was then inserted into an autoclave steel capsule and transferred to an electric oven and incubated at 250 °C for 3 days. The mixture was cooled to room temperature, and a white precipitate of AlTp was separated from the solution. The precipitate was rinsed several times with deionized water to remove byproducts and unreacted materials, and then it was dried in air at room temperature. To remove terephthalic acid and water molecules that are unreacted and encapsulated within the cavities of the AlTp, the product was calcined for 72 h at 360 °C under air.

To prepare CrTp, 13.7 mmol from $Cr(NO_3)_3.9H_2O$ was mixed with 14 mmol terephthalic acid in about 70 ml distilled water, and the reaction proceeded as described above. To synthesize BiTp, 2 mmol terephthalic acid was dissolved in 15 ml DMF and then added dropwise to 20 ml DMF solution of 1.33 mmol $Bi(NO_3)_3.5H_2O$. The synthesis was completed as explained above, and the final product was washed and dried for further usages.

3.3. Corrosion tests

Electrochemical impedance spectroscopy (EIS) measurements were carried out by using an Autolab PGSTAT30 in a cell with the three electrodes of Ag/AgCl (3M KCl), AM60B sheet, and platinum wire as the reference, working, and counter electrodes, respectively in stagnant condition. The frequency range was from 10 kHz to 10 mHz with an AC voltage of 5.0 mV. Potentiodynamic polarization was measured by the same cell in a potential range of −250 to 250 mV versus open circuit potential at a scan rate of 1 mV s^{-1}. The immersion time before all measurements was about 2 h. Corrosion tests were carried out on the Mg alloy specimens with a size of 1×1 cm and composition of Al:5.5-6.5%, Mn:0.24-0.6%, Zn:0.22%, and Si:0.1%, which were abraded with a series of emery papers and then washed with double-distilled water, degreased with acetone, and dried in air.

4. Conclusion

Three terephthalate-based MOFs were successfully synthesized under hydrodynamic conditions. SEM images revealed that the prepared MOFs had different morphologies, which affected their inhibition abilities. Such different structures resulted in different active surface areas, as demonstrated by BET results. Corrosion tests indicated that all the proposed components exhibited inhibition efficiency higher than 84%, which could be considered as potential inhibitors in ethylene glycol + water solution as the coolant of magnesium engine blocks. It was also found that CrTp with an inhibition efficiency of about 90% exhibited better performance than BiTp and AlTp. Gibbs free energy of adsorption showed that the studied inhibitors were adsorbed on the AM60B surface by a mixed process of chemisorption and physisorption.

Acknowledgements

Financial support by Tabriz Branch, Islamic Azad University is gratefully acknowledged.

References

[1] D. S. Kumar, C. T. Sasanka, K. Ravindra, and K. N. S. Suman, Magnesium and its alloys in automotive applications–a review, Am. J. Mater. Sci. Technol 4 (2015) 12–30.

[2] G. Song, Corrosion and its inhibition of engine block magnesium alloys in coolants, 2001.

[3] G. Song, and D. StJohn, Corrosion behaviour of magnesium in ethylene glycol, Corros. Sci. 46 (2004) 1381–1399.
[4] E. Slavcheva, G. Petkova, and P. Andreev, Inhibition of corrosion of AZ91 magnesium alloy in ethylene glycol solution in presence of chloride anions, Mater. Corros. 56 (2005) 83–87.
[5] H. Ashassi-Sorkhabi, S. Moradi-Alavian, R. Jafari, A. Kazempour, and E. Asghari, Effect of amino acids and montmorillonite nanoparticles on improving the corrosion protection characteristics of hybrid sol-gel coating applied on AZ91 Mg alloy, Mater. Chem. Phys. 225 (2019) 298–308.
[6] H. Ashassi-Sorkhabi, S. Moradi-Alavian, M. D. Esrafili, and A. Kazempour, Hybrid sol-gel coatings based on silanes-amino acids for corrosion protection of AZ91 magnesium alloy: Electrochemical and DFT insights, Prog. Org. Coatings 131 (2019) 191–202.
[7] H. Ashassi-Sorkhabi, S. Moradi-Alavian, and A. Kazempour, Salt-nanoparticle systems incorporated into sol-gel coatings for corrosion protection of AZ91 magnesium alloy, Prog. Org. Coatings 135 (2019) 475–482.
[8] M. A. Ashraf, Z. Liu, W.-X. Peng, and N. Yoysefi, Amino acid and TiO2 nanoparticles mixture inserted into sol-gel coatings: An efficient corrosion protection system for AZ91 magnesium alloy, Prog. Org. Coatings 136 (2019) 105296.
[9] S. Pirsa, F. Asadzadeh, and I. K. Sani, Synthesis of magnetic gluten/pectin/Fe 3 O 4 Nano-hydrogel and its use to reduce environmental pollutants from lake Urmia sediments, J. Inorg. Organomet. Polym. Mater. 30 (2020) 3188–3198.
[10] S. Mostafavi, V. Rezaverdinejad, and S. Pirsa, Design and fabrication of nanocomposite-based polyurethane filter for improving municipal waste water quality and removing organic pollutants, Adsorpt. Sci. Technol. 37 (2019) 95–112.
[11] M. A. Sheikh-Mohseni, and S. Pirsa, Nanostructured Conducting Polymer/Copper Oxide as a Modifier for Fabrication of L-DOPA and Uric Acid Electrochemical Sensor, Electroanalysis 28 (2016) 2075–2080.
[12] L. Wang, T. Zhou, and J. Liang, Corrosion and self-healing behaviour of AZ91D magnesium alloy in ethylene glycol/water solutions, Mater. Corros. 63 (2012) 713–719.
[13] A. M. Fekry, and M. Z. Fatayerji, Electrochemical corrosion behavior of AZ91D alloy in ethylene glycol, Electrochim. Acta 54 (2009) 6522–6528.
[14] N. Alizadeh, S. Pirsa, A. Mani-Varnosfaderani, and M. S. Alizadeh, Design and fabrication of open-tubular array gas sensors based on conducting polypyrrole modified with crown ethers for simultaneous determination of alkylamines, IEEE Sens. J. 15 (2015) 4130–4136.
[15] J. Yan, S. Jiang, S. Ji, D. Shi, and H. Cheng, Metal-organic framework MIL-53 (Al): synthesis, catalytic performance for the Friedel-Crafts acylation, and reaction mechanism, Sci. China Chem. 58 (2015) 1544–1552.
[16] X. Zhao, X. Xiong, X. Chen, J. Hu, and J. Li, Synthesis of halide anion-doped bismuth terephthalate hybrids for organic pollutant removal, Appl. Organomet. Chem. 30 (2016) 304–310.
[17] M. S. Alivand, M. Shafiei-Alavijeh, N. H. M. H. Tehrani, E. Ghasemy, A. Rashidi, and S. Fakhraie, Facile and high-yield synthesis of improved MIL-101 (Cr) metal-organic framework with exceptional CO2 and H2S uptake; the impact of excess ligand-cluster, Microporous Mesoporous Mater. 279 (2019) 153–164.
[18] T. Zhao, F. Jeremias, I. Boldog, B. Nguyen, S. K. Henninger, and C. Janiak, High-yield, fluoride-free and large-scale synthesis of MIL-101 (Cr), Dalt. Trans. 44 (2015) 16791–16801.
[19] A. Jmiai, B. El Ibrahimi, A. Tara, R. Oukhrib, S. El Issami, O. Jbara, L. Bazzi, and M. Hilali, Chitosan as an eco-friendly inhibitor for copper corrosion in acidic medium: protocol and characterization, Cellulose 24 (2017) 3843–3867.
[20] M. Gobara, S. Elbasuney, A. Baraka, H. Kamal, M. Elsayed, and E. A. McNally, Novel Smart Hydroxyapatite/Silica Sol–Gel Nanocomposite Hybrid Coating for Corrosion Protection of AA2024, J. Inorg. Organomet. Polym. Mater. 28 (2018) 1598–1608.
[21] H. Ashassi-Sorkhabi, and M. Es'haghi, Electro-synthesis of nano-colloidal PANI/ND composite for enhancement of corrosion-protection effect of PANI coatings, J. Mater. Eng. Perform. 22 (2013) 3755–3761.
[22] A. Majedi, F. Davar, A. Abbasi, and A. Ashrafi, Modified sol–gel based nanostructured zirconia thin film: preparation, characterization, photocatalyst and corrosion behavior, J. Inorg. Organomet. Polym. Mater. 26 (2016) 932–942.
[23] B. El Ibrahimi, A. Jmiai, K. El Mouaden, A. Baddouh, S. El Issami, L. Bazzi, and M. Hilali, Effect of solution's pH and molecular structure of three linear α-amino acids on the corrosion of tin in salt solution: A combined experimental and theoretical approach, J. Mol. Struct. 1196 (2019) 105–118.
[24] A. E.-A. S. Fouda, S. E.-D. H. Etaiw, M. M. El-bendary, and M. M. Maher, Metal-organic frameworks based on silver (I) and nitrogen donors as new corrosion inhibitors for copper in HCl solution, J. Mol. Liq. 213 (2016) 228–234.
[25] S. E. H. Etaiw, A. E.-A. S. Fouda, S. N. Abdou, and M. M. El-bendary, Structure, characterization and inhibition activity of new metal–organic framework, Corros. Sci. 53 (2011) 3657–3665.
[26] S. Saker, N. Aliouane, H. Hammache, S. Chafaa, and G. Bouet, Tetraphosphonic acid as eco-friendly corrosion inhibitor on carbon steel in 3% NaCl aqueous solution, Ionics (Kiel). 21 (2015) 2079–2090.
[27] M. Es'haghi, A. Amjad, S. Asghari, and A. Lotfi, Studying effect of plantain extract behavior as an eco-friendly corrosion inhibitor on the mild steel in 1 M HCl solution, Anti-Corrosion Methods Mater. (2018).
[28] A. Jmiai, B. El Ibrahimi, A. Tara, S. El Issami, O. Jbara, and L. Bazzi, Alginate biopolymer as green corrosion inhibitor for copper in 1 M hydrochloric acid: experimental and theoretical approaches, J. Mol. Struct. 1157 (2018) 408–417.
[29] H. Ashassi-Sorkhabi, and A. Kazempour, Thermodynamic and kinetic insights into the role of amino acids in improving the adhesion of iota-carrageenan as a natural corrosion inhibitor to the aluminum surface, J. Adhes. Sci. Technol. (2019) 1–15.
[30] A. Addoun, S. Bouyegh, M. Dahmane, O. Ferroukhi, and M. Trari, Thermodynamic investigation on the adhesion and corrosion inhibition properties of a non-steroidal anti-inflammatory drug in HCl electrolyte applied on mild steel material, Mater. Today Commun. 21 (2019) 100720.
[31] M. Ouakki, M. Galai, M. Rbaa, A. S. Abousalem, B. Lakhrissi, E. H. Rifi, and M. Cherkaoui, Investigation of imidazole derivatives as corrosion inhibitors for mild steel in sulfuric acidic environment: experimental and theoretical studies, Ionics (Kiel). (2020) 1–22.